

Time-Reversal-Invariant Hofstadter-Hubbard Model with Ultracold Fermions

Daniel Cocks,^{1,*} Peter P. Orth,^{2,*} Stephan Rachel,^{3,4} Michael Buchhold,¹ Karyn Le Hur,^{3,5} and Walter Hofstetter¹

¹*Institut für Theoretische Physik, Goethe-Universität, 60438 Frankfurt/Main, Germany*

²*Institute for Theory of Condensed Matter, Karlsruhe Institute of Technology (KIT), 76131 Karlsruhe, Germany*

³*Department of Physics, Yale University, New Haven, Connecticut 06520, USA*

⁴*Institute for Theoretical Physics, Dresden University of Technology, 01062 Dresden, Germany*

⁵*Center for Theoretical Physics, Ecole Polytechnique, CNRS, 91128 Palaiseau Cedex, France*

We consider the time-reversal-invariant Hofstadter-Hubbard model which can be realized in cold atom experiments. In these experiments, an additional staggered potential and an artificial Rashba-type spin-orbit coupling are available. Without interactions, the system exhibits various phases such as topological and normal insulator, metal as well as semi-metal phases with two or even more Dirac cones. Using a combination of real-space dynamical mean-field theory and analytical techniques, we discuss the effect of on-site interactions and determine the corresponding phase diagram. In particular, we investigate the semi-metal to antiferromagnetic insulator transition and the stability of different topological insulator phases in the presence of strong interactions. We compute spectral functions which allow us to study the edge states of the strongly correlated topological phases.

PACS numbers: 67.85-d, 37.10.Jk

Introduction.— Ultracold quantum gases trapped in optical lattice potentials provide insight into strongly correlated condensed matter systems. Examples are the Mott-insulator-superfluid transition, the dynamics of the Hubbard model after a quench of parameters, and the simulation of quantum magnetism [1]. Striking is the precise experimental control over almost all system parameters, including the particle-particle interaction strength. Simulating more traditional electronic condensed matter systems, however, is complicated by the fact that cold atoms are charge neutral, and their center of mass motion is thus not affected by external magnetic or electric fields (apart from trapping potentials). An experimental breakthrough was thus the engineering of so-called “artificial” gauge fields, which give rise to effective magnetic or electric fields for the neutral particles [2]. Remarkably, they may even be generalized to simulate spin-orbit couplings or non-Abelian fields [3]. The effective electromagnetic fields and couplings can be large, which allows, for example, realization of the quantum (spin) Hall effect in a completely new experimental context [4–8].

The underlying idea of realizing time-reversal-invariant two-dimensional (2D) topological phases with cold atoms is as simple as it is fundamental [5, 7]. Consider the (integer) quantum Hall effect (QHE) on a 2D square lattice where an external magnetic field along the z direction breaks time-reversal and translational symmetry. The single particle spectrum for arbitrary magnetic field strength – having the shape of a butterfly – was first computed by Douglas Hofstadter [9] since then referred to as the *Hofstadter butterfly*. If the magnetic flux per plaquette is a rational number $\alpha = p/q$, in units of the Dirac flux quantum $\Phi_0 = h/e$, the system remains translationally invariant with an enlarged unit cell of q lattice sites. The spectrum consists of q energy bands and in all energy gaps one finds a finite Chern number C and

correspondingly $|C|$ chiral edge modes per edge. Interestingly, for even values of q the system is a semi-metal at half-filling and exhibits q Dirac cones.

To restore time-reversal symmetry we can imagine applying a magnetic field in the z direction that only couples to the up-spins and a second field of the same strength but opposite direction that only couples to the down-spins. We thus end up with a spinful and time-reversal-invariant (TRI) version of the fundamental Hofstadter problem. Remarkably, such a scenario is feasible using cold atoms in artificial gauge fields [7, 8]. Thus, the semi-metallic Dirac dispersion for even q becomes a generalization of graphene with a tunable number of Dirac cones. Energy gaps which were crossed by a single chiral edge mode in the QHE setup are now traversed by a helical Kramer’s pair of edge states, corresponding to a topological insulator phase. Note that one can use the same Gedanken experiment to construct the Kane–Mele model [4] from two time-reversed copies of Haldane’s honeycomb model [10]. The Kane–Mele model with additional Hubbard interaction has recently been intensively studied [11], in contrast to the Hofstadter problem.

In this Letter we study the effect of interactions in the (TR-invariant) *Hofstadter-Hubbard model* using real-space dynamical mean-field theory (RDMFT) [12]. We explain our numerical results using analytical arguments. We consider interaction effects on both (semi-)metallic and gapped topological phases. Although \mathbb{Z}_2 topological insulators are known to be robust against disorder [13, 14], rigorous and general results about the fate of topological insulators in the presence of Coulomb or Hubbard interactions are limited [15]. Some three-dimensional materials of the iridate family are possible candidates for systems where strong spin–orbit coupling and Coulomb interactions compete [16, 17]. In two dimensions, however, topological insulator phases

have so far only been found in HgTe/CdTe quantum wells [18, 19], where Coulomb interactions seem to be negligible.

Interacting TRI Hofstadter problem.— The TRI Hofstadter-Hubbard model is described by the Hamiltonian

$$H = - \sum_j \left\{ t_x c_{j+\hat{x}}^\dagger c_j + t_y c_{j+\hat{y}}^\dagger e^{i2\pi\alpha x \sigma^z} c_j + \text{h.c.} \right\} + \sum_j U n_{j,\uparrow} n_{j,\downarrow}, \quad (1)$$

where $c_j^\dagger = (c_{j\uparrow}^\dagger, c_{j\downarrow}^\dagger)$ at lattice site $j = (x, y)$, σ^z is a Pauli matrix and $\hat{x} = (1, 0)$, $\hat{y} = (0, 1)$ are unit vectors. t_x (t_y) is the hopping amplitude in x (y) direction. We focus on isotropic hopping $t_x = t_y = t$ here, and express all energies in units of $t \equiv 1$. The value of α determines the strength of the (artificial) magnetic field for either spin species which penetrates a lattice plaquette in units of the Dirac flux quantum. The on-site interaction strength U can be experimentally tuned by Feshbach resonances and by adjusting the lattice depth. For $U = 0$ this model was studied in Ref. 7 (for experimental details see Supplemental Material).

We first consider the TRI Hofstadter-Hubbard problem for general $\alpha = p/q$ at half filling. For q odd the system is metallic with a nested Fermi surface, and antiferromagnetic Néel order occurs for infinitesimally small interaction $U = 0^+$ as for the ordinary square lattice. For q even the situation is very different because the system is a semimetal (SM) at half filling [20]. The noninteracting

band structure exhibits q Dirac cones (with a multiplicity of 2 due to spin) which are separated by momentum $2\pi/q$ in momentum space. The $\alpha = 1/2$ case is thus very similar to graphene (but note that the coordination number is $z = 4$ rather than $z = 3$). For smaller α on the other hand the system embodies a generalization of graphene with a tunable number of valleys.

We investigate the SM-insulator transition for various $\alpha = 1/q$ (q even) within RDMFT. In Fig. 1, the magnetization is shown as a function of interaction U . The insulating phase for $U > U_c$ is antiferromagnetically (AFM) ordered with a magnetization pointing in the z -direction and an ordering wave vector $\mathbf{Q} = (\pi, \pi)$. We find that the critical value of U_c to enter the insulating and magnetically ordered phase decreases for increasing q . This is expected from the increased scattering that can take place between the cones. At U_c we also observe a simultaneous opening of the single particle gap. Within our approach we thus find no sign of an intermediate non-magnetic gapped phase.

To understand the behavior of $U_c(q)$ we make use of Herbut's argument [21]. Herbut considers graphene and studies the SM-insulator transition within a large- N approach, and finds that U_c depends on $2N$, the number of Dirac cones (N refers to the spin degeneracy), and the Fermi velocity v_F as $U_c \sim v_F/2N$. As shown in detail in the Supplemental Material, we are able to match our results with Herbut's analysis by replacing the Fermi velocities and $2N = qN$. In fact, from the bandstructure at $U = 0$ we find $v_F \propto 1/q$. Consequently, setting $N = 2$ for spin-1/2 particles, U_c should exhibit a $1/q^2$ behavior which agrees very well with the RDMFT data; see inset of Fig. 1. We further note that we find that $U_c(\alpha = 3/8) < U_c(\alpha = 1/8)$, which is in agreement with the analysis above since $v_F(\alpha = 3/8) < v_F(\alpha = 1/8)$.

Specific cold atom setup.— We now consider two additional terms in the Hamiltonian that are available in the cold-atom setup [7, 8]: a staggering of the optical lattice

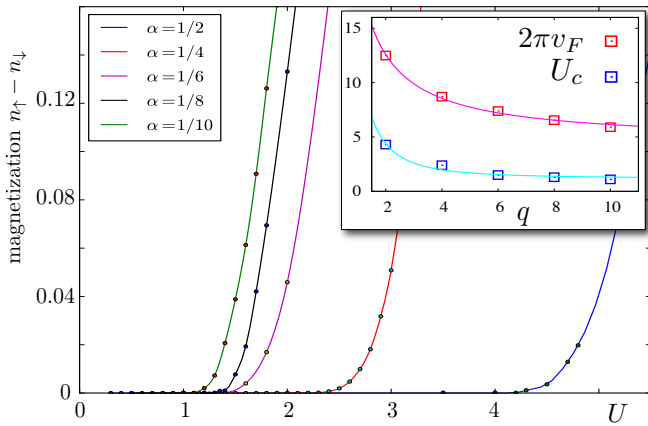


FIG. 1. (color online). Magnetization $m = n_\uparrow - n_\downarrow$ in the Néel state is plotted versus interaction strength U . We show results for $\alpha = 1/2$ (blue), $1/4$ (red), $1/6$ (magenta), $1/8$ (black), and $1/10$ (green) (curves from left to right). Inset: Fermi velocity $2\pi v_F$ (red symbols) for different $\alpha = 1/q$ is shown versus q . U_c (blue symbols) obtained within RDMFT versus q is also shown. Magenta (upper) line is a fit of v_F to $\propto 1/q$ and cyan (lower) line of U_c to $\propto 1/q^2$. Note that odd q denominators exhibit $U_c = 0^+$ due to a nested Fermi surface.

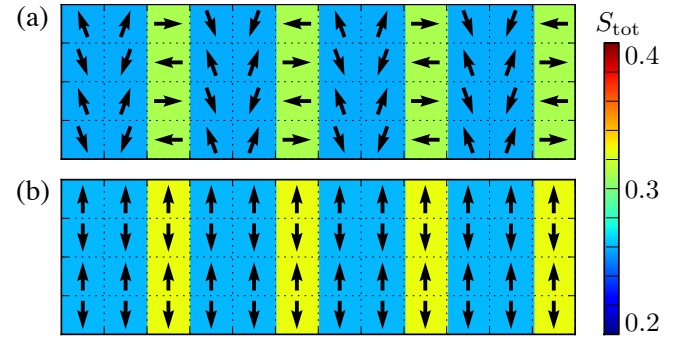


FIG. 2. (color online). Real space magnetization profile $\mathbf{m}(\mathbf{x})$ in S^y - S^z plane for $\alpha = 1/6$, $U = 5$, $\lambda_x = 0$, and $\gamma = 0.125$ (a) and $\gamma = 0.25$ (b), respectively.

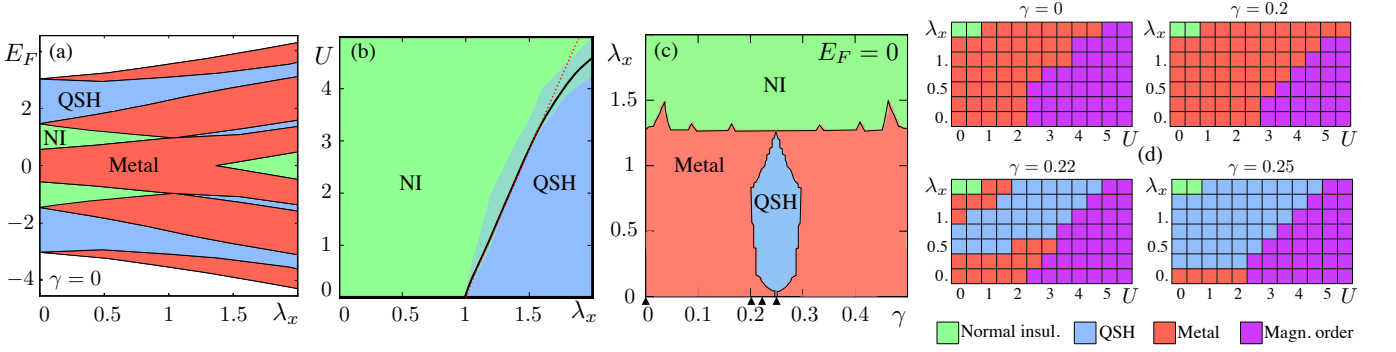


FIG. 3. (color online). (a) E_F - λ_x -phase diagram at $\gamma = U = 0$. (b) U - λ_x -phase diagram at $n_F = 2/3$ and $\gamma = 0$. (c) λ_x - γ -phase diagram at half filling $n_F = 1$ and $U = 0$. (d) U - λ_x -phase diagrams at $E_F = 0$ for various values of γ [indicated by arrows in part (c)] and inverse temperature $\beta = 20$. We find (semi)metal (red), normal insulator (NI) (green, in upper left), topological insulator (QSH) (blue), and magnetically ordered phases (purple, in lower right).

potential along the x direction

$$H_\lambda = \sum_j (-1)^x \lambda_x c_j^\dagger c_j, \quad (2)$$

and a Rashba-like spin-orbit coupling that breaks axial spin symmetry. It is introduced via replacing in Eq. (15)

$$t_x \rightarrow t_x \exp(-i2\pi\gamma\sigma^x). \quad (3)$$

We first study the effect of finite λ_x and γ on the magnetic ordering.

Tunable magnetism.— For $\gamma = 0$, increasing λ_x increases U_c but does not change the type of magnetic order. Finite γ does, however, change the type of magnetic order in general. To demonstrate this we consider fixed $U = 5$ at $\alpha = 1/6$ and calculate the magnetization in real space for various values of $\gamma \in [0, 0.25]$. The spin operators are defined in terms of the fermionic operators as usual as $\mathbf{S}_j = \frac{1}{2} c_j^\dagger \boldsymbol{\sigma} c_j$ with $\boldsymbol{\sigma} = (\sigma^x, \sigma^y, \sigma^z)$. We show the magnetization pattern for $\gamma = 0.125$ and $\gamma = 0.25$ in Fig. 2 obtained within RDMFT. We obtain similar results for other values of α and γ . For $\gamma = 0.125$, the magnetization lies in the S^y - S^z plane, has a periodicity of six (two) lattice sites along x (y) and reads explicitly $\mathbf{m}(\mathbf{x}) = S_{\text{tot}}(x) \cos \pi y (0, -\cos(\frac{\pi x}{3} + \eta), \sin(\frac{\pi x}{3} + \eta))$ with $\eta = 0.39 \sin \frac{\pi x}{3} \cos \frac{\pi x}{3}$. The magnetization makes angles of $\{0^\circ, 70^\circ, 110^\circ, 180^\circ, 250^\circ, 290^\circ\}$ in the S^y - S^z plane (spiral order). For $\gamma = 0.25$, the magnetic order is given by $\mathbf{m}(\mathbf{x}) = S_{\text{tot}}(x)(0, 0, \cos \pi y)$ (collinear order). Quantum fluctuations reduce the size of the magnetization $S_{\text{tot}} < 1/2$, which depends not only on the parameters α, γ and U/t , but is also spatially staggered for intermediate values of U/t (see Fig. 2). The staggering decreases for larger values of U/t . More importantly, tuning the parameter γ we pass from Néel to spiral to collinear order crossing two magnetic quantum phase transitions.

We can qualitatively understand this type of magnetic order by rigorously deriving a quantum spin Hamiltonian

for even stronger interactions when charge fluctuations freeze out at half filling (see Supplemental Material for details)

$$\begin{aligned} \mathcal{H} = & J_x \sum_j \left\{ S_j^x S_{j+\hat{x}}^x + \cos(4\pi\gamma) \left[S_j^y S_{j+\hat{x}}^y + S_j^z S_{j+\hat{x}}^z \right] \right. \\ & \left. + \sin(4\pi\gamma) \left[S_j^z S_{j+\hat{x}}^y - S_j^y S_{j+\hat{x}}^z \right] \right\} \\ & + J_y \sum_j \left\{ \cos(4\pi\alpha) \left[S_j^x S_{j+\hat{y}}^x + S_j^y S_{j+\hat{y}}^y \right] + S_j^z S_{j+\hat{y}}^z \right. \\ & \left. + \sin(4\pi\alpha) \left[S_j^y S_{j+\hat{y}}^x - S_j^x S_{j+\hat{y}}^y \right] \right\} \end{aligned} \quad (4)$$

where $J_i = 4t_i^2/U$. The first part describes spin exchange in x direction. For $\gamma = n/2$ with $n \in \mathbb{Z}$ we obtain a simple antiferromagnetic Heisenberg term. Other values of γ , however, break $SU(2)$ symmetry and cause anisotropy of the XXZ type with S^x as anisotropy direction in spin space. For $\gamma \neq n/4$ there is an additional Dzyaloshinskii-Moriya (DM) interaction term in the YZ plane, which is responsible for the spiral spin order in Fig. 2(a). Spin exchange in the y direction is periodic with an extended unit cell in the x direction depending on the flux $\alpha = p/q$: for odd q the unit cell contains q lattice sites, but for even q it only contains $q/2$ lattice sites, reflecting second order perturbation theory. For instance, one finds for the π -flux lattice ($\alpha = 1/2$) an ordinary Heisenberg exchange term. For other values of α the XY term exhibits a modulation of its amplitude depending on α , while the Z term always favors AFM Ising order. The rich magnetic order predicted by the spin Hamiltonian is in agreement with our RDMFT findings.

Topological insulators.— Let us now turn to the study of interaction effects on the gapped phases. For $U = 0$, we distinguish the normal (NI) and topological (TI) insulating phases by calculating the \mathbb{Z}_2 invariant ν using Hatsugai's method [22]. For $U > 0$, we identify the

phases by computing the spectral function in a cylindrical geometry using RDMFT and counting the number of gapless helical edge states crossing the bulk gap (for technical details we refer to the Supplemental Material). The TI phase exhibits an odd number of helical Kramer's pairs per edge while the NI phase an even number (including zero). Edge states are also crucial for detection of topological phases in cold-atom experiments, and we numerically study how robust they are with respect to interactions. In the following, we focus on fixed $\alpha = 1/6$, which qualitatively captures all phenomena that occur in this system for general $\alpha = p/q$.

In the axial symmetric case of $\gamma = 0$ there exist TI phases only away from half filling, since the system is a (semi)metal for $n_F = 1$ (and not too large λ_x, U). This is shown in Fig. 3(a), and is expected as the spinless Hofstadter problem at $\alpha = 1/6$ exhibits a QHE with Chern number $C = \pm 2$ for E_F in the two energy gaps closest to zero and a QHE with $C = \pm 1$ for E_F in the other gaps. The Chern number corresponds to the number of chiral edge modes in an open geometry. In the present time-reversal invariant system we thus find an according number of helical Kramer's pairs within the gaps.

For a filling of $n_F = 1/3, 5/3$ the system is thus a TI. We observe this topological phase to be stable even for large interactions up to $U = 10$. We can induce a NI-TI phase transition in the other gap for $n_F = 2/3, 4/3$ by applying a large enough staggered lattice potential $\lambda_x \geq 1$ [see Fig. 3(a)]. Fixing $n_F = 2/3$ we now turn on interactions, and observe that this phase is quite stable as shown in Fig. 3(b). Eventually, large enough interactions reverse the effect of the staggering potential and drive the system into the NI phase. Note that a static Hartree-like approximation (red dashed line) yields comparable results for small U but overestimates the effect of staggering for larger values of U .

A topological phase at half filling occurs only if we break the axial symmetry in the system by considering $\gamma > 0$. We present the non-interacting λ_x - γ phase diagram in Fig. 3(c) [7]. The interacting λ_x - U phase diagram for different values of γ is shown in Fig. 3(d). Both semimetal and QSH phases are robust up to interactions of order $U \simeq 3 - 5$, at which point larger interactions drive the system into a magnetically ordered state. Prominently, we observe an interaction-driven NI to QSH transition for $\gamma = 0.25$ and $\lambda_x \gtrsim 1.5$, and a metal-QSH transition for $0.22 \leq \gamma < 0.25$ and $\lambda_x \gtrsim 1$.

Using RDMFT for a cylinder geometry, we are able to directly observe the behavior of the edge states in the interacting system. Gapless edge states are key to different detection schemes of topological phases in cold-atom systems [23, 24]. Since topological phases are uniquely characterized by their helical edge states [25], a probe of these states is the most direct measurement [7, 26]. In Fig. 4, we give an example of the spectral function $A(k_y, \omega)$ for the interaction driven NI-QSH transition at

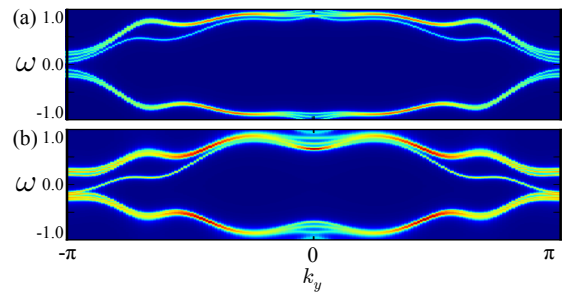


FIG. 4. (color online). Spectral function $A(k_y, \omega)$ of interacting system clearly distinguishing between (a) NI phase with no edge states traversing the bulk gap at $U = 0.5$ and (b) QSH phase at $U = 2$ with a single pair of edge modes (per edge) connecting the two bulk bands. Both plots are for $\alpha = 1/6$, $\gamma = 0.25$ and $\lambda_x = 1.5$.

$\gamma = 0.25$, $\lambda_x = 1.5$. For $U = 0.5$, we find no gapless edge modes that are connecting the two bulk bands, corresponding to NI, while at $U = 2$ we clearly find a single pair of helical edge modes traversing the bulk gap, which corresponds to the QSH phase.

Conclusion.— We have investigated the TRI Hofstadter-Hubbard model using RDMFT complemented by analytical arguments. We quantitatively determine the interacting phase diagram including two additional terms available in the cold-atom experiment, a lattice staggering and Rashba-type spin-orbit coupling. Interactions drive various phase transitions. Similar to graphene, we find that a semi-metal at half-filling turns into a magnetic insulator at a critical finite interaction strength. Rashba-type spin-orbit interactions lead to tunable magnetic order with collinear and spiral phases. We explicitly demonstrate the stability of the topological phases with respect to interactions, and verify the existence of robust helical edge states in the strongly correlated TI phase, which is crucial for experimental detection schemes.

Note added.— After the submission of this work a number of other studies appeared [27] that investigate the strong-coupling limit of fermions (and bosons) in the presence of non-Abelian gauge fields using a spin Hamiltonian similar to our Eq. (4).

The authors acknowledge useful discussions with L. Fritz, K. Sengstock, and I. Spielman. This work was supported by the DFG under Grant No. RA 1949/1-1 (S.R.) and via Sonderforschungsbereich SFB-TR/49 and Forschergruppe FOR 801 (D.C., M.B., W.H.), by the NSF under NSF DMR 0803200 (K.L.H.), and the Young Investigator Group of P.P.O. received financial support from the “Concept for the Future” of the KIT within the framework of the German Excellence Initiative. K.L.H. and W.H. benefitted from a summer conference at the Aspen Center for Physics supported by the NSF under Grant No. 1066293. D.C. and P.P.O. contributed equally to this work.

* These authors contributed equally to this work.

- [1] W. S. Bakr *et al.*, Science **329**, 547 (2010); U. Schneider *et al.*, Nat. Phys. **8**, 213 (2012); J. Simon *et al.*, Nature **472**, 307 (2011).
- [2] J. Dalibard *et al.*, Rev. Mod. Phys. **83**, 1523 (2011); R. Dum and M. Olshanii, Phys. Rev. Lett. **76**, 1788 (1996); J. Ruostekoski *et al.*, Phys. Rev. Lett. **88**, 180401 (2002); D. Jaksch and P. Zoller, New J. Phys. **5**, 56 (2003); G. Juzeliunas and P. Öhberg, Phys. Rev. Lett. **93**, 033602 (2004); E. J. Mueller, Phys. Rev. A **70**, 041603(R) (2004); Y.-J. Lin *et al.*, Nature **462**, 628 (2009); M. Aidelsburger *et al.*, Phys. Rev. Lett. **107**, 255301 (2011); K. Jimenez-Garcia *et al.*, Phys. Rev. Lett. **108**, 225303 (2012); N. Cooper, Phys. Rev. Lett. **106**, 175301 (2011).
- [3] A. M. Dudarev *et al.*, Phys. Rev. Lett. **92**, 153005 (2004); K. Osterloh *et al.*, Phys. Rev. Lett. **95**, 010403 (2005); J. Ruseckas *et al.*, Phys. Rev. Lett. **95**, 010404 (2005); I. I. Satija *et al.*, Phys. Rev. Lett. **97**, 216401 (2006); N. Goldman, EPL **80**, 20001 (2007); I. I. Satija *et al.*, Phys. Rev. A **77**, 043410 (2008); Y.-J. Lin *et al.*, Nature **471**, 83 (2011); J. Struck *et al.*, Phys. Rev. Lett. **108**, 225304 (2012); L. Cheuk *et al.*, Phys. Rev. Lett. **109**, 095302 (2012); P. Wang *et al.*, Phys. Rev. Lett. **109**, 095301 (2012); P. Hauke *et al.*, Phys. Rev. Lett. **109**, 145301 (2012).
- [4] C. L. Kane and E. J. Mele, Phys. Rev. Lett. **95**, 146802 (2005); *ibid.* **95**, 226801 (2005).
- [5] B. A. Bernevig and S. C. Zhang, Phys. Rev. Lett. **96**, 106802 (2006).
- [6] M. Z. Hasan and C. L. Kane, Rev. Mod. Phys. **82**, 3045 (2010); X.-L. Qi and S.-C. Zhang, Rev. Mod. Phys. **83**, 1057 (2011).
- [7] N. Goldman *et al.*, Phys. Rev. Lett. **105**, 255302 (2010).
- [8] F. Gerbier and J. Dalibard, New J. Phys. **12**, 033007 (2010).
- [9] D. R. Hofstadter, Phys. Rev. B **14**, 2239 (1976).
- [10] F. D. M. Haldane, Phys. Rev. Lett. **61**, 2015 (1988).
- [11] S. Rachel and K. Le Hur, Phys. Rev. B **82**, 075106 (2010); M. Hohenadler, T. C. Lang, and F. F. Assaad, Phys. Rev. Lett. **106**, 100403 (2011); D. Soriano, J. Fernandez-Rossier, Phys. Rev. B **82**, 161302 (2010); D. Zheng, C. Wu and Z. Zhong, Phys. Rev. B **84**, 205121 (2011); S.-L. Yu, X. C. Xie, and J.-X. Li, Phys. Rev. Lett. **107**, 010401 (2011); D.-H. Lee, Phys. Rev. Lett. **107**, 166806 (2011); W. Wu, S. Rachel, W.-M. Liu, and K. Le Hur, Phys. Rev. B **85**, 205102 (2012); A. Rüegg and G. Fiete, Phys. Rev. Lett. **108**, 046401 (2012); C. Griset and C. Xu, Phys. Rev. B **85**, 045123 (2012); M. Hohenadler *et al.*, Phys. Rev. B **85**, 115132 (2012); M. Mardani, M.-S. Vaezi, and A. Vaezi, arXiv:1111.5980.
- [12] A. Georges, G. Kotliar, W. Krauth, and M. J. Rozenberg, Rev. Mod. Phys. **68**, 13 (1996); M. Snoek, I. Titvinidze, C. Töke, K. Byczuk, and W. Hofstetter, New J. Phys., **10**, 093008 (2008); R. Bulla *et al.*, Rev. Mod. Phys. **80**, 395 (2008); E. Gull *et al.*, Rev. Mod. Phys. **83**, 349 (2011).
- [13] J. E. Moore and L. Balents, Phys. Rev. B **75**, 121306(R) (2007).
- [14] A. P. Schnyder *et al.*, Phys. Rev. B **78**, 195125 (2008); E. Prodan, T. L. Hughes, and B. A. Bernevig, Phys. Rev. Lett. **105**, 115501 (2010).
- [15] C. Xu and J. E. Moore, Phys. Rev. B **73**, 045322 (2006); M. Levin and A. Stern, Phys. Rev. Lett. **103**, 196803 (2009); Z. Wang, X.-L. Qi, and S.-C. Zhang, *ibid.* **105**, 256803 (2010); V. Gurarie, Phys. Rev. B **83**, 085426 (2011); J. C. Budich *et al.*, arXiv:1203.2928.
- [16] D. A. Pesin and L. Balents, Nature Phys. **6**, 376 (2010).
- [17] M. Kargarian, J. Wen, and G. A. Fiete, Phys. Rev. B **83**, 165112 (2011).
- [18] B. A. Bernevig, T. L. Hughes, and S.-C. Zhang, Science **314**, 1757 (2006).
- [19] M. König *et al.*, Science **318**, 766 (2007).
- [20] M. Kohmoto, Phys. Rev. B **39**, 11943 (1989).
- [21] I. F. Herbut, Phys. Rev. Lett. **97**, 146401 (2006).
- [22] T. Fukui and Y. Hatsugai, Phys. Rev. B **75**, 121403 (2007).
- [23] T. D. Stanescu *et al.*, Phys. Rev. A **79**, 053639 (2009); T. D. Stanescu *et al.*, *ibid.* **82**, 013608 (2010); H. M. Price and N. R. Cooper, *ibid.* **85**, 033620 (2012); X.-J. Liu *et al.*, *ibid.* **81**, 033622 (2010); B. Béri and N. R. Cooper, Phys. Rev. Lett. **107**, 145301 (2011).
- [24] R. O. Umucalilar *et al.*, Phys. Rev. Lett. **100**, 070402 (2008); E. Zaho *et al.*, Phys. Rev. A **84**, 063629 (2011); E. Alba *et al.*, Phys. Rev. Lett. **107**, 235301 (2011).
- [25] C. Wu, B. A. Bernevig, and S.-C. Zhang, Phys. Rev. Lett. **96**, 106401 (2006);
- [26] N. Goldman, J. Beugnon, and F. Gerbier, Phys. Rev. Lett. **108**, 255303 (2012). M. Buchhold, D. Cocks, and W. Hofstetter, Phys. Rev. A **85**, 063614 (2012).
- [27] M. Gong *et al.*, arXiv:1205.6211; W. S. Cole *et al.*, Phys. Rev. Lett. **109**, 085302 (2012); J. Radic *et al.*, Phys. Rev. Lett. **109**, 085303 (2012); Z. Cai *et al.*, Phys. Rev. A **85**, 061605(R) (2012).

EXPERIMENTAL DETAILS

Realizations

We investigate a model Hamiltonian implementing a non-Abelian artificial gauge field in a fermionic system. This model system is of general interest to topological insulator experiments, and directly applicable to cold-gas systems in optical lattices, of which a wealth of proposals have been made to implement these artificial gauge fields [1].

Cold-gas experiments can exhibit effective Hamiltonians with artificial gauge fields through two main methods: geometric phases or rotation of the cold-gas system. A geometry phase is created when a spatially dependent coupling connects states of an atom such that the Aharonov-Bohm effect is observed in the adiabatic passage of the atom in one particular dressed state through a closed loop [1]. The first such realization of a geometrically induced artificial gauge field was performed within a continuous cold-gas of bosonic ^{87}Rb with a pair of Raman lasers and a spatially varying magnetic field [4]. Alternatively, the Hamiltonian of a rotation system can be expressed in the rotating frame, and one finds it is time-independent when the system is isotropic and introduces Coriolis terms that take the form of an artificial gauge [2]. Such rotating systems have been achieved in the laboratory, with features such as a vortex lattice structure [3] appearing in bosonic systems.

In a lattice, one can also introduce additional couplings in order to create a continuous flux and the so-called “optical flux lattice” has been proposed [5] to realize topological non-trivial systems. However, it is not necessary to realize an artificial gauge over the entire lattice. Instead, one can make use of the Peierls’ substitution [6], which results in a tight-binding model that differs only by a phase factor in either the hopping matrix elements or, equivalently, of the local Wannier states. This phase factor, the Peierls’ phase, can be realized by “freezing out” the hopping in a lattice and then reconnecting the lattice sites by an additional coupling as first proposed by [7]. Such a realization of an Abelian artificial gauge field for a square lattice geometry has already been achieved in [8] by coupling columns of ^{87}Rb in a staggered optical lattice with Raman couplings, where the artificial magnetic flux alternates in sign between neighboring plaquettes. An extension of such a lattice to simulate a net magnetic flux, which exhibits quantum Hall phases, is proposed in [9] via the inclusion of a super-lattice potential. Similarly, [10, 11] have shown that it is possible to generate non-Abelian gauge fields by asymmetric lattice shaking and the extension of any Abelian gauge field in a cold-gas experiment to a non-Abelian gauge field is possible by the use of an n -state atomic system [12]. The specific proposal which we follow, Goldman *et al.* [13], makes use of

this idea by manipulating four states of ^6Li to implement a non-Abelian gauge field such that a $\text{SU}(2)$ time-reversal invariant form of the Hofstadter model is realized. With this setup, it is possible to realize any rational flux ratio $\alpha = p/q < 1/2$. For large α , the edge states associated with these have been reported [13] to be robust for deviations in the flux of up to $\Delta\alpha \sim 0.01$. In addition, the non-Abelian nature of the gauge field realizes a spin-orbit coupling, which is the γ term in our Hamiltonian, introduced in equation (3). This term has a similar effect as the Rashba spin-orbit coupling in the related Kane-Mele system [14], a model that is closely related to graphene. Many other proposals exist for spin-orbit coupling in continuous ultracold gases [15–17] which could also be extended to lattice geometries.

Detection and Trapping

The major differences between cold-gas and solid-state experiments are the mechanisms that are available to observe the topological properties and edge-states of the system, as well as the size and structure of the edge that is present. In optical lattices, it is not possible to perform transport measurements for the Hall coefficients, and so one must turn to other options to directly observe these states. Several proposals have been made that use techniques such as Bragg or Raman spectroscopy [18–20], which directly detect the edge states and can be applied regardless of the trapping potential, time-of-flight measurements [21] to determine bulk properties, and direct band mapping by the use of spin-injection spectroscopy [17].

We have investigated detection using Bragg spectroscopy in [18] for the non-interacting version of the system considered in this paper. While it is in principle possible for us to determine the Bragg response via RDMFT results, we have not observed a qualitative change of the single-particle spectra corresponding to the edge states. Hence, we do not expect a qualitative deviation in Bragg response for excitations of these edge states compared to the non-interacting system.

HERBUT’S ARGUMENT

In Fig. 1(a) in the main text we presented numerical RDMFT results for the critical onsite interaction strength $U_c(1/q)$ which marks a zero temperature quantum phase transition between a semi-metallic phase and a magnetically ordered phase. The system develops a single-particle gap inside the magnetic phase. The magnetic order is antiferromagnetic and of Néel type.

In this section, we expand our analytical analysis of the critical value of U_c which we obtain from a slightly modified version of Herbut’s argument. In Ref. [22] I. Herbut

considers the low energy field theory of graphene in the presence of onsite interaction U . Specifically, graphene exhibits four Dirac cones at low energies, a factor of two stemming from the two valleys (K, K') and a factor of two stemming from the electronic spin. In his renormalization group analysis, Herbut extends the electronic spin from two to N_s flavors and determines the β -function of the Hubbard interaction to leading order in $1/N_s$. In his notation, it reads

$$\beta_a = -\tilde{g}_a - C_a \tilde{g}_a^2 + \mathcal{O}(1/N_s), \quad (5)$$

where $\tilde{g}_a = g_a \frac{2}{N_s}$ and $g_a = -U/(8\pi\tilde{v}_F t)$ with hopping amplitude t and dimensionless Fermi velocity $\tilde{v}_F = v_F/at$. Here, a is the short distance cutoff of the theory that is set such that the Fermi velocity $v_F = \tilde{v}_F at = 1$. The constant in the β -function reads $C_a = 2N_v$, where N_v is the number of different valleys. For graphene, one finds that $N_v = 2$, but in the spinful Hofstadter system one rather finds that $N_v = q$ and so depends on the magnetic flux per unit cell $\alpha = p/q$. The critical value of the interaction U_c is obtained from the condition that the β -function changes sign, which yields

$$(g_a)_c = \frac{-2}{C_a N_s} = \frac{-2}{2q N_s}. \quad (6)$$

In terms of the microscopic parameters this reads

$$\left(\frac{U}{t}\right)_c = \frac{16\pi\tilde{v}_F}{2qN_s} = \frac{4\pi\tilde{v}_F}{q}, \quad (7)$$

where we have inserted the physical value of $N_s = 2$, in our Hofstadter model. The Fermi velocity $\tilde{v}_F(q)$ is exactly known from the non-interacting band structure of the Hofstadter model, and we find that it scales as $\tilde{v}_F(q) \sim 1/q$ for $\alpha = 1/q$ in the considered range $2 \leq q \leq 10$ [see inset in Fig. 1(a)]. As a result, we predict that

$$\left(\frac{U}{t}\right)_c \sim \frac{1}{q^2} \quad (8)$$

which agrees very well with the numerical RDMFT results as we show in the inset of Fig. 1(a).

DERIVATION OF EFFECTIVE SPIN HAMILTONIAN

In the main text we introduce the fermionic tight-binding Hamiltonian including interactions and in the presence of the two gauge fields along the x and y links, which reads $H = H_0 + H_I$ with

$$H_0 = - \sum_j \left\{ t_x c_{j+\hat{x}}^\dagger e^{-i2\pi\gamma\sigma^x} c_j + t_y c_{j+\hat{y}}^\dagger e^{i2\pi\alpha x\sigma^z} c_j + \text{h.c.} \right\} \quad (9)$$

$$H_I = U \sum_j n_{j,\uparrow} n_{j,\downarrow}. \quad (10)$$

The summation $j = (x, y)$ with $x, y \in \mathbb{N}$ runs over all lattice sites of the square lattice with lattice constant set to one. The field operator $c_j^\dagger = (c_{j,\uparrow}^\dagger, c_{j,\downarrow}^\dagger)$ is a spinor.

At large interaction, the zeroth order Hamiltonian is given by the interaction part H_I . To pursue perturbation theory in the hopping amplitudes $t_{x,y}$ and derive an effective spin Hamiltonian at half-filling up to $\mathcal{O}(t_{x,y}^2/U)$, we follow the analysis in Ref. 23 and partition the complete Fock space into states with singly occupied sites

$$S = \{|n_{1\uparrow}, n_{1\downarrow}, n_{2\uparrow}, \dots\rangle : \forall i : n_{i\uparrow} + n_{i\downarrow} \leq 1\} \quad (11)$$

and states with at least one doubly occupied site

$$D = \{|n_{1\uparrow}, n_{1\downarrow}, n_{2\uparrow}, \dots\rangle : \exists i : n_{i\uparrow} + n_{i\downarrow} = 2\}. \quad (12)$$

We partition the Hamiltonian as

$$H = \begin{pmatrix} A & B \\ C & D \end{pmatrix} = \begin{pmatrix} P_S H P_S & P_S H P_D \\ P_D H P_S & P_D H P_D \end{pmatrix}, \quad (13)$$

where $P_S(P_D)$ projects onto the subspace $S(D)$. The effective Hamiltonian in the low-energy subspace S is obtained by projecting the resolvent operator $G(E) = (E - H)^{-1}$ on this subspace $P_S G(E) P_S = [E - \mathcal{H}(E)]^{-1}$ with $\mathcal{H}(E) = A + B \frac{1}{E-D} C$. Expanding to lowest order in $t_{x,y}/U$ and E/U yields the (energy independent) low-energy effective Hamiltonian

$$\mathcal{H} = P_S H_0 P_S + P_S H_0 P_D \left(-\frac{1}{U} \sum_j n_{j\uparrow} n_{j\downarrow} \right) P_D H_0 P_S. \quad (14)$$

At half-filling the first term $P_S H_0 P_S$ vanishes, because starting from subspace S each hopping event of H_0 creates a doubly occupied site and the projection onto S yields zero. It requires at least two hopping events for the system to return to the singly-occupied subspace S . The second term in Eq. (14) contains all possible second-order virtual hopping events. Inserting the hopping Hamiltonian H_0 in Eq. (14) and defining the 2×2 complex hopping matrices $T_{\hat{x}} = t_x \exp(-i2\pi\gamma\sigma^x)$ and $T_{\hat{y}}(x) = t_y \exp(i2\pi\alpha x\sigma^z)$, the effective Hamiltonian can be written as

$$\mathcal{H} = -\frac{1}{U} P_S \left[\sum_{j,k} \sum_{\nu, \mu \in \{\pm\hat{x}, \pm\hat{y}\}} (\nu, \mu)_{j,k} \right] P_S. \quad (15)$$

Here, $\hat{x} = (1, 0)$, $\hat{y} = (0, 1)$ are unit vectors and

$$(\nu, \mu)_{j,k} = c_{j+\nu}^\dagger T_\nu c_j c_{k+\mu}^\dagger T_\mu c_k. \quad (16)$$

Note that the hopping matrices fulfill $T_{-\nu} = T_\nu^*$. To arrive at Eq. (15) we have also employed that $P_D \sum_j n_{j,\uparrow} n_{j,\downarrow} P_D = 1$, since exactly one site is doubly occupied in the system after the first hopping event.

To proceed, we use that the system must return to the singly occupied sector S after the second hopping event.

Otherwise, the state is annihilated by the projection operator P_S . It follows that only terms with $\nu = -\mu$ in the sum in Eq. (15) are non-zero. For $\nu = -\mu = \pm\hat{x}$, this demands that $k = j \pm \hat{x}$ in Eq. (16). Explicitly, we find (up to constants)

$$\begin{aligned} (\hat{x}, -\hat{x}) &= t_x^2 \sum_{\substack{j;\sigma,\sigma' \\ \tau,\tau'}} c_{j+\hat{x},\sigma}^\dagger [\delta_{\sigma\sigma'} \cos(2\pi\gamma) - i\sigma_{\sigma\sigma'}^x \sin(2\pi\gamma)] \\ &\quad \times c_{j,\sigma'} c_{j,\tau}^\dagger [\delta_{\tau\tau'} \cos(2\pi\gamma) + i\sigma_{\tau\tau'}^x \sin(2\pi\gamma)] c_{j+\hat{x},\tau'} \\ &= -2t_x^2 \sum_j \{ \cos(4\pi\gamma) (S_{j+\hat{x}}^y S_j^y + S_{j+\hat{x}}^z S_j^z) \\ &\quad + \sin(4\pi\gamma) (S_{j+\hat{x}}^z S_j^y - S_{j+\hat{x}}^y S_j^z) + S_{j+\hat{x}}^x S_j^x \}, \end{aligned} \quad (17)$$

where the spin indices $\sigma, \sigma', \tau, \tau' \in \{\uparrow, \downarrow\}$ and we have defined the spin operators $\mathbf{S}_j = \frac{1}{2} \sum_{\tau\tau'} c_{j,\tau}^\dagger \boldsymbol{\sigma}_{\tau\tau'} c_{j,\tau'}$ with $\boldsymbol{\sigma} = (\sigma^x, \sigma^y, \sigma^z)$. We have used the relation

$$\sum_{\sigma,\tau} c_{j,\sigma}^\dagger c_{k,\sigma} c_{k,\tau}^\dagger c_{j,\tau} = -2\mathbf{S}_j \cdot \mathbf{S}_k - \frac{1}{2} n_j n_k + n_j, \quad (18)$$

where $n_j = 1$ in our case. Since Eq. (17) is purely real, its hermitian conjugate term $(-\hat{x}, \hat{x})$ is identical to it. Similarly, we obtain for virtual hopping along the y -direction

$$\begin{aligned} (2, -2) &= -2t_y^2 \sum_j \{ \cos(4\pi\alpha x) (S_{j+\hat{y}}^x S_j^x + S_{j+\hat{y}}^y S_j^y) \\ &\quad + \sin(4\pi\alpha x) (S_{j+\hat{y}}^z S_j^y - S_{j+\hat{y}}^y S_j^z) + S_{j+\hat{y}}^z S_j^z \} \end{aligned} \quad (19)$$

where $j = (x, y)$. The complete low-energy spin Hamiltonian thus reads

$$\begin{aligned} \mathcal{H} &= \frac{1}{U} \sum_{\nu \in \{\pm\hat{x}, \pm\hat{y}\}} (\nu, -\nu) \\ &= \frac{t_x^2}{U} \sum_j \left\{ S_j^x S_{j+\hat{x}}^x + \cos(4\pi\gamma) [S_j^y S_{j+\hat{x}}^y + S_j^z S_{j+\hat{x}}^z] \right. \\ &\quad \left. + \sin(4\pi\gamma) [S_j^z S_{j+\hat{x}}^y - S_j^y S_{j+\hat{x}}^z] \right\} \\ &\quad + \frac{t_y^2}{U} \sum_j \left\{ \cos(4\pi\alpha x) [S_j^x S_{j+\hat{y}}^x + S_j^y S_{j+\hat{y}}^y] + S_j^z S_{j+\hat{y}}^z \right. \\ &\quad \left. + \sin(4\pi\alpha x) [S_j^y S_{j+\hat{y}}^x - S_j^x S_{j+\hat{y}}^y] \right\}, \end{aligned} \quad (20)$$

which is the result given in Eq. (4) of the main text.

NUMERICAL METHOD DETAILS

RDMFT details

We have used the real-space dynamical mean-field theory (RDMFT) [24] to investigate numerically the effects

of weak, intermediate and strong interactions. RDMFT operates on a finite realization of a lattice by the Dyson equation:

$$[G^{-1}]_{ij} = [G^0]_{ij}^{-1} - \Sigma_{ij} \quad (21)$$

where i and j refer to single sites of the system, G^0 is the non-interacting Green's function, and we adopt a vector notation, such that each site is decomposed into its spin-dependent components:

$$G_{ij} = \begin{bmatrix} G_{\uparrow\uparrow,ij} & G_{\uparrow\downarrow,ij} \\ G_{\downarrow\uparrow,ij} & G_{\downarrow\downarrow,ij} \end{bmatrix}, \quad (22)$$

and similarly with the other Green's functions and self-energy. The core assumption of RDMFT, as with standard DMFT, is that the self-energy is local $\Sigma_{ij} = \Sigma_i \delta_{ij}$.

In the RDMFT procedure, we map each site onto an impurity problem by integrating out all other degrees of freedom in the lattice. To solve the impurity problem we use a combination of exact diagonalization (ED), numerical renormalization group (NRG) [25] and the continuous-time auxiliary spin solver (CT-AUX) [26]. The NRG solver operates directly at $T = 0$ and in real-frequency, which we use for the cases where $\gamma = 0$. The ED and CT-AUX solvers operate in Matsubara frequencies and at finite temperature. These solvers are well known in solving the system without the spin-mixing due to the γ term in Hamiltonian (1), and we make some comments about the inclusion of spin-mixing below.

To directly observe edge states in our system, we must take a finite system and enforce cylindrical boundary conditions. That is, we set periodic boundary conditions in the y direction and open (i.e. fixed) boundary conditions in the x direction. In this case, we can assume k_y is a good quantum number when no symmetry breaking has occurred. We investigate system sizes up to 48 sites in the x -direction and have allowed for symmetry breaking with a periodicity of up to 24 sites in the y -direction. Because we have observed no other symmetry breaking than AF order in the y -direction, we are able to restrict the number of impurity solver calculations to that of the lattice size in the x -direction. We also investigate the periodic system to better determine the onset of magnetism without boundary effects.

Solver details

To extend the standard Anderson impurity model to include spin-orbit coupling we must include, at minimum, a term that couples the bath orbitals of opposite spins to the impurity. The complete Hamiltonian for the impurity

is then given by

$$H_{AIM} = - \sum_{\sigma} \mu c_{\sigma}^{\dagger} c_{\sigma} + \sum_{l\sigma} \epsilon_{l\sigma} a_{l\sigma}^{\dagger} a_{l\sigma} \quad (23)$$

$$+ \sum_{l\sigma} \left[V_{l\sigma} a_{l\sigma}^{\dagger} c_{\sigma} + W_{l\sigma} a_{l\bar{\sigma}}^{\dagger} c_{\sigma} + h.c. \right] + U n_{\uparrow} n_{\downarrow},$$

where c_{σ} is an impurity annihilation operator, $a_{l\sigma}$ is a bath annihilation operator, and $\bar{\sigma}$ represents the opposite spin to σ . Here, the term involving $W_{l\sigma}$ represents the extension of the impurity model. Due to this term, the Weiss Green's functions for the impurity model become:

$$\mathcal{G}_{\sigma\sigma}^{-1}(i\omega_n) = i\omega_n + \mu - \sum_l \left[\frac{|V_l|^2}{i\omega_n - \epsilon_{l\sigma}} + \frac{|W_l|^2}{i\omega_n - \epsilon_{l\bar{\sigma}}} \right] \quad (24)$$

$$\mathcal{G}_{\sigma\bar{\sigma}}^{-1}(i\omega_n) = - \sum_l \left[\frac{V_{l\sigma}^* W_{l\bar{\sigma}} + W_{l\sigma}^* V_{l\bar{\sigma}}}{i\omega_n - \epsilon_{l\sigma}} \right]. \quad (25)$$

Formally, the CT-AUX solver is unchanged by the inclusion of the spin-mixing, however one must now also track the spin-mixing Weiss Green's functions, $\mathcal{G}_{\sigma\bar{\sigma}}$, for each configuration of auxiliary spins. This means that the fast-matrix updates for the solver [26] become rank-2 updates. In addition, we were unable to prove that the determinants which must be evaluated will always be real, and so we must consider the possibility of a “sign problem” (or more precisely, a phase problem) in the Monte-Carlo sampling. However, we have carefully analyzed all of our results and observed purely real and positive weights for all configurations that we consider.

Details about gaps and magnetization

From our converged RDMFT solutions, we determine several quantities directly from the output of the impurity solvers, including magnetization, double occupancy and the density of states at the Fermi edge for each site of the lattice. To identify the phase, we observe the presence of a charge gap via several methods: a zero density of states at the Fermi edge, determined from extrapolation of the Matsubara Green's functions to $\omega = 0$, an exponential decay of the imaginary time Green's functions, which is fitted to the form $G(\tau) \sim \exp(-\tau\Delta_{\text{sp}})$, and the analytical continuation [27] to a real-frequency spectrum, by first continuing the self-energy [28].

In each case, we extract trends for different system size and temperature to determine the properties of the infinite system at low temperatures. However, we do not wish to claim exact results for $T = 0$ data, as this is beyond the capabilities of our solver, and therefore explicitly show the results for $\beta = 20$. We have compared

these results to that of $\beta = 50$ for some cases and do not notice significant changes in the critical interactions for magnetic transitions.

In our system we observe two different phase transitions in the presence of interactions: a) Semi-metal to magnetic order. In this transition, we observe a simultaneous opening of the single-particle gap and magnetic order throughout the entire lattice, and b) Quantum spin-Hall phase to magnetic order. Here the system always possesses a single-particle gap in the bulk, and so the only noticeable change in the bulk is the onset of magnetic order. Near the edge, the topological edge states also become gapped in this transition, however at larger temperatures we observe the single-particle gap opening later than the appearance of magnetization. As the magnetization has destroyed time-reversal symmetry, these states will be susceptible to disorder and localize. The fate of these states in ultracold atom experiments is unknown and requires further investigation.

* These authors contributed equally to this work.

- [1] J. Dalibard *et al.*, Rev. Mod. Phys. **83**, 1523 (2011).
- [2] A. Fetter, Rev. Mod. Phys. **81**, 647 (2009).
- [3] J. R. Abo-Shaeer *et al.*, Phys. Rev. Lett. **88**, 070409 (2001).
- [4] Y. Lin *et al.*, Nature **462**, 628 (2009).
- [5] N. Cooper, Phys. Rev. Lett. **106**, 175301 (2011).
- [6] D. Hofstadter, Phys. Rev. B **14**, 2239 (1976).
- [7] D. Jaksch and P. Zoller, New J. Phys. **5**, 56 (2003).
- [8] M. Aidelsburger *et al.*, Phys. Rev. Lett. **107**, 255301 (2011).
- [9] F. Gerbier and J. Dalibard, New J. Phys. **12**, 033007 (2010).
- [10] J. Struck *et al.*, Phys. Rev. Lett. **108**, 225304 (2012).
- [11] P. Hauke *et al.*, Phys. Rev. Lett. **109**, 145301 (2012).
- [12] K. Osterloh *et al.*, Phys. Rev. Lett. **95**, 010403 (2005).
- [13] N. Goldman *et al.*, Phys. Rev. Lett. **105**, 255302 (2010).
- [14] W. Wu *et al.*, Phys. Rev. B **85**, 205102 (2012).
- [15] B. Anderson *et al.*, Phys. Rev. Lett. **108**, 235301 (2012).
- [16] Campbell *et al.*, Phys. Rev. A **84**, 025602 (2011).
- [17] L. Cheuk *et al.*, Phys. Rev. Lett. **109**, 095302 (2012).
- [18] M. Buchhold *et al.*, Phys. Rev. A **85**, 063614 (2012).
- [19] N. Goldman *et al.*, Phys. Rev. Lett. **108**, 255303 (2012).
- [20] X. Liu *et al.*, Phys. Rev. A **81**, 033622 (2010).
- [21] E. Alba *et al.*, Phys. Rev. Lett. **107**, 235301 (2011).
- [22] I. F. Herbut, Phys. Rev. Lett. **97**, 146401 (2006).
- [23] A. Auerbach, *Interacting electrons and quantum magnetism* (Springer-Verlag, New York, 1994).
- [24] M. Snoek *et al.*, New J. Phys. **10**, 093008 (2008).
- [25] R. Bulla *et al.*, Phys. Rev. B **64**, 45103 (2001).
- [26] E. Gull *et al.*, Rev. Mod. Phys. **83**, 349 (2011).
- [27] M. Jarrell and J.E. Gubernatis, Phys. Rep. **269**, 133 (1996).
- [28] X. Wang *et al.*, Phys. Rev. B **80**, 045101 (2009).